nature geoscience

LETTERS

PUBLISHED ONLINE: 17 FEBRUARY 2013 | DOI: 10.1038/NGEO1731

Strong increase in convective precipitation in response to higher temperatures

Peter Berg[1,2], Christopher Moseley[3,4] and Jan O. Haerter[5]*

Precipitation changes can affect society more directly than variations in most other meteorological observables[1–3], but precipitation is difficult to characterize because of fluctuations on nearly all temporal and spatial scales. In addition, the intensity of extreme precipitation rises markedly at higher temperature[4–9], faster than the rate of increase in the atmosphere's water-holding capacity[1,4], termed the Clausius–Clapeyron rate. Invigoration of convective precipitation (such as thunderstorms) has been favoured over a rise in stratiform precipitation (such as large-scale frontal precipitation) as a cause for this increase[4,10], but the relative contributions of these two types of precipitation have been difficult to disentangle. Here we combine large data sets from radar measurements and rain gauges over Germany with corresponding synoptic observations and temperature records, and separate convective and stratiform precipitation events by cloud observations. We find that for stratiform precipitation, extremes increase with temperature at approximately the Clausius–Clapeyron rate, without characteristic scales. In contrast, convective precipitation exhibits characteristic spatial and temporal scales, and its intensity in response to warming exceeds the Clausius–Clapeyron rate. We conclude that convective precipitation responds much more sensitively to temperature increases than stratiform precipitation, and increasingly dominates events of extreme precipitation.

The Clausius–Clapeyron relation describes the rate of change of saturation vapour pressure of approximately 7% $^{\circ}C^{-1}$ at typical surface temperatures, and thereby sets a scale for increases in precipitation extremes[1]. Recent studies on extreme precipitation have indeed found that high precipitation percentiles on short observational timescales generally increase with temperature[4–9,11]. For the Netherlands, increases of extreme precipitation intensity roughly commensurate with the Clausius–Clapeyron rate at low temperatures but beyond this rate at temperatures above 12 °C were first reported in 2008 (ref. 4). Remarkably, similar observations were subsequently made for other mid-latitude[7,9] and tropical regions[8,9] for short timescales. However, the difficulty of identifying precipitation types[12,13]—namely stratiform and convective rain—and relatively limited data[11] have made unequivocal attribution of the high rate above 12 °C to either of the types unfeasible. Even statistical effects have been suggested to explain the super-Clausius–Clapeyron rate[11,14].

The basic hypothesis is that precipitation intensity changes may be tied to the change in saturation vapour pressure. It hinges on the assumption that precipitation intensity should be proportional to changes in the mixing ratio at cloud base. Everything else held constant, condensation should increase accordingly. Atmospheric temperature changes may however alter other quantities—such as the moist adiabatic lapse rate—thereby affecting the actual rate of condensation[15–17].

With persistent uncertainties and dependence on parameterizations in precipitation simulated by global climate models[18–20], a promising path towards a better statistical characterization of precipitation are convection-resolving models. Although no support for intensity increases beyond the Clausius–Clapeyron rate was gained from some studies[15,16], others found that extreme rainfall at high temperatures may increase beyond the Clausius–Clapeyron rate, when the life cycle of individual storms is monitored[10]. The difficulty in reaching final agreement on the mechanism of the scaling with temperature in simulations[10,15,16] may partially be due to their idealized set-up, acting on relatively small scales. Observed variability in the mesoscale and synoptic conditions, required as atmospheric boundary conditions, cannot be fully taken into account. These uncertainties call for direct observational demonstration of the scaling for the different types.

Precipitation is most directly measured by ground-based gauges. We use a large, temporally and spatially dense network of gauges in southwestern Germany (Fig. 1a), comprising 90 gauges with five-minute temporal resolution over an eight-year-long time period. This provides approximately 700 years of aggregated data. The gauge data are complemented by extensive radar measurements, providing five-minute instantaneous radar reflectivity fields covering Germany (Fig. 1a) over two years. All precipitation records are matched with daily temperature measurements for the corresponding time periods.

Convective and stratiform types are separated using three-hourly synoptic observations over Germany (Fig. 1a). At any given time, the precipitation measurements from both data sets are separated into convective and stratiform types depending on the observed clouds[11]. Examples are depicted in Fig. 1b,c (see Methods for details).

Figure 2a shows the intensity distribution function for both precipitation types for the five-minute temporal intervals (gauge records). Only non-zero ($\geq$0.1 mm/5 min) measurements were used, corresponding to approximately 3% of the data (see Supplementary Fig. S2d). The stratiform type shows power-law behaviour for intensities above 4 mm h^{-1}, with an exponent $\gamma \approx -3$. This implies a well-defined mean but divergent higher-order statistics of the distribution. Conversely, for convective precipitation, the distribution follows a completely different

[1]Institute for Meteorology and Climate Research, Karlsruhe Institute of Technology, Wolfgang-Gaede-Weg 1, 76131 Karlsruhe, Germany, [2]Rossby Centre, Swedish Meteorological and Hydrological Institute, Folkborgsvägen 17, 6017631 Norrköping, Sweden, [3]Max Planck Institute for Meteorology, Bundesstraße 53, 20146 Hamburg, Germany, [4]Helmholtz Zentrum Geesthacht, Climate Service Center, Fischertwiete 1, 200956 Hamburg, Germany, [5]Center for Models of Life, Niels Bohr Institute, University of Copenhagen, Blegdamsvej 17, 2100 Copenhagen, Denmark. *e-mail: haerter@nbi.dk.

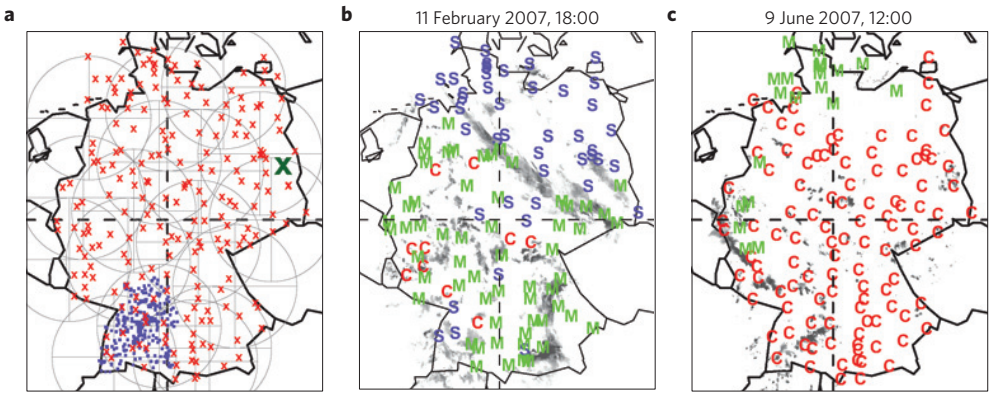

Figure 1 | Separation of precipitation types. a, Map of the investigation area with radar (grey circles), synoptic (red crosses) and precipitation gauge stations (blue dots). The quadrants used for the radar processing are shown as dashed lines. The Lindenberg station for comparison with the bright-band method (see Methods) is marked with a bold green cross. **b**, Example of a dominant stratiform synoptic weather condition. The symbols S and M mark observations of stratiform and mixed synoptic cloud conditions, respectively radar-observed rain intensity is marked as grey shades. **c**, The same as for **b** but for dominant convective (C) conditions.

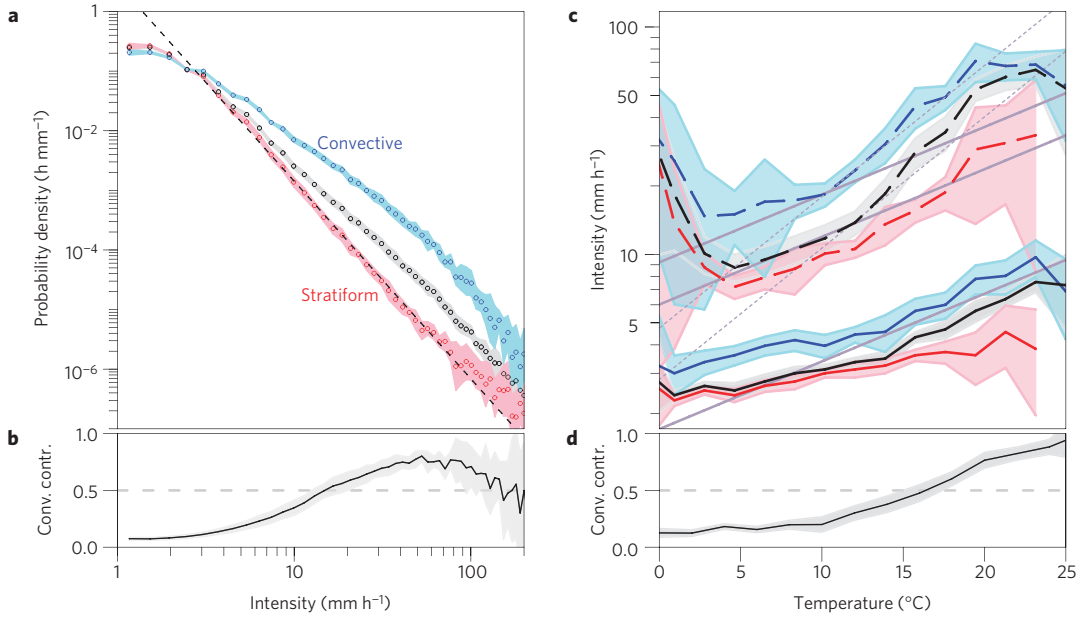

Figure 2 | Probability distribution of precipitation intensity. a, Five-minute precipitation intensity distribution for convective (blue), stratiform (red) and total precipitation (black) from gauges. Dashed line: power-law fit (log–log axes). **b**, The relative contribution of convective precipitation to the sum of the two types of precipitation as a function of intensity (logarithmic horizontal scale). **c**, Intensity percentiles of convective (blue), stratiform (red) and total precipitation (black) for the 75th (solid) and 99th (long-dashed) percentiles. Solid and dashed purple lines mark 7% °C^{-1} and 14% °C^{-1} increases, respectively (logarithmic vertical axis). **d**, The same as for **b** but as a function of temperature. Shaded areas denote the 90% confidence intervals computed by bootstrapping.

dependency on intensity. In this log–log plot, the convective curve is concave, that is, steeper at higher intensities. Note also that total observed precipitation (all data used) deviates only slightly from a power-law behaviour at moderate intensities. This is due to the dominance of the stratiform type in the total statistics for those intensities (Fig. 2b). The concavity of the curve of convective precipitation has the effect that the convective contribution grows with increasing intensity only until a certain point, around 70 mm h^{-1}, after which it decays.

When binning by temperature, stratiform and convective precipitation also show different characteristics (Fig. 2c). Percentiles of both types generally increase with temperature. However, whereas no statistically significant exceedance of the Clausius–Clapeyron rate is found for the stratiform type, the higher percentiles of convective precipitation substantially exceed this rate above approximately 10 °C. Total precipitation (steeply increasing above approximately 12 °C) is transitional between the stratiform and convective types as the relative contribution shifts from one to the other as a function of temperature (Fig. 2d), and can thus even exceed the increase of the types individually[11,14]. The statistics for hourly total precipitation percentiles (Supplementary Fig. S3) agrees with previous results[4,8]. The decreasing slope above approximately 22 °C is a signature of the convective distribution (Fig. 2a), and seems to be a stable high-temperature feature of convection[7,8]. Using radar data (Supplementary Fig. S4), a super-Clausius–Clapeyron increase is also found for convection, but not for stratiform precipitation.

For society, the statistical intensity distributions in Fig. 2 may not be of concern, as long as extremes are limited to short

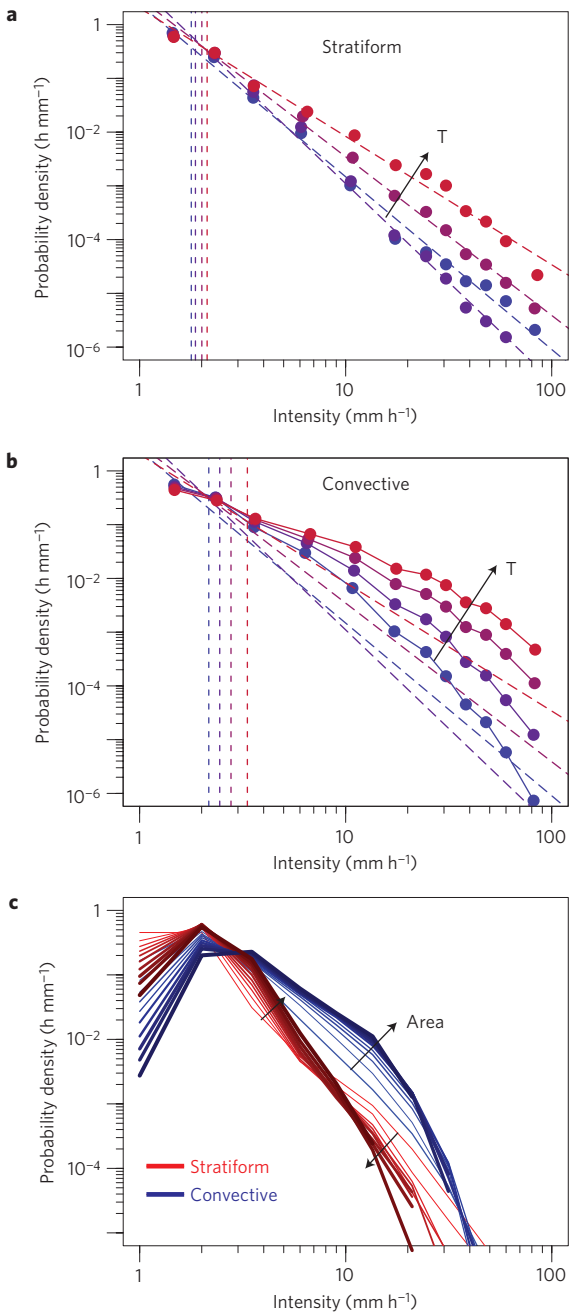

Figure 3 | Event intensity profile and correlations. a, Intensity distributions of stratiform events with areas 100–400 km^2 for temperatures 2.5–22.5 °C from radar data. Increasing temperatures (5 °C steps) are shown in colours from blue to red. **b**, The same as for **a** but for convection. Dashed lines are power-law fits to curves in **a**. Vertical dashed lines indicate distribution means. **c**, Distribution of event-mean intensity conditional on area. Blue and red shades denote convective and stratiform precipitation, respectively. Areas range from 10–400 km^2 (thin to thick lines). Arrows indicate increasing area. Note log–log axes.

durations. Actual precipitation occurs in events that can be defined as sequences of contiguous observations in space or time. Event statistics more directly reflect the life cycle of precipitation in convective plumes or large-scale fronts—information that is concealed in fixed-interval statistics.

Using radar records, we consider the distribution of precipitation intensity within events of a given area. For any given temperature, stratiform precipitation events (Fig. 3a) approximately follow power-law distributions that become broader at high temperatures. Note that changes in the power-law exponent with temperature entail rapid increases of extremes, but relatively small increases in the mean. Convective precipitation (Fig. 3b) overall does not follow such power-law behaviour. The distributions are flatter for low intensities but decrease more rapidly at high intensities. Both extremes and means increase much more rapidly as a function of temperature. These differences in intensity distributions have important implications for extreme events: sampling randomly—that is, composing an uncorrelated event—from the distributions in Fig. 3a,b would lead to rapid drift of the resulting event mean intensity towards the overall mean; however, real events have temporally and spatially correlated intensities. Such correlations can cause events to produce persistent heavy precipitation[21], which can be devastating to human lives and infrastructure.

We now contrast the distribution functions of convective and stratiform average event intensity. For a meaningful comparison, we bin the data so that only events of similar area are compared—curves of equal thickness in Fig. 3c. Stratiform precipitation exhibits a crossover of curves with increasing area at around 10 mm h^{-1}. This crossover can be seen as a signature of sampling randomly from intensity distributions (see also Supplementary Fig. S6). It indicates that larger events produce more moderate average precipitation intensity than smaller events. Conversely, convective precipitation shows no sign of such a crossover up to the highest observed intensities. Hence, even the mean of convective events becomes more intense when their area increases. These results are consistent with a characteristic, spatially correlated intensity profile of convective cells[22,23].

Events occur in space and time. An observer at a fixed location perceives the event as a temporal sequence of intensities of a given duration, whereas for watershed management, flood control and operational forecasting the spatial extent of events is also relevant[24]. Figure 4 shows that the statistics of the two observers can be made compatible. Consider first the fixed observer (gauge records): the occurrence frequencies of stratiform and convective events both decay rapidly with increasing durations (Fig. 4a). The convective type, however, is concave and falls off faster for longer durations, whereas the stratiform type follows a nearly straight line on the log–log scale. Similar behaviour is detected in the radar data (spatial observer) as a function of the event size (Fig. 4c). The two distributions in Fig. 4a,c in fact approximately map onto each other when event area is taken as proportional to the square of duration. This is intuitively plausible as observed durations of travelling rain cells should scale as the diameter. Mean and extreme event intensities increase with duration and area (Fig. 4d,f). However, for convection, the curves saturate near 30 min durations and areas of 100 km^2, a reflection of their plume-like cross-section. Weighting the distributions in Fig. 4a by duration and corresponding intensities (Fig. 4d), the precipitation yield—that is, total amount generated—at any given duration is obtained (Supplementary Fig. S7a,c). Unlike stratiform precipitation, the predominant yield of convective events occurs for events of intermediate duration, or area.

Finally, we return to the temperature dependence, but for events of a given duration (Fig. 4b,e). Stratiform events have no pronounced temperature dependence (Fig. 4e), with increases ranging below those of the fixed interval statistics (Fig. 2c). Conversely, convective events as a whole produce intensity increases beyond the Clausius–Clapeyron rate for extreme events, supporting a recent modelling study[10]. These results should be seen in the light of increased convective contributions to total precipitation (Fig. 4b and Supplementary Fig. S7b) at higher temperatures (above approximately 14 °C).

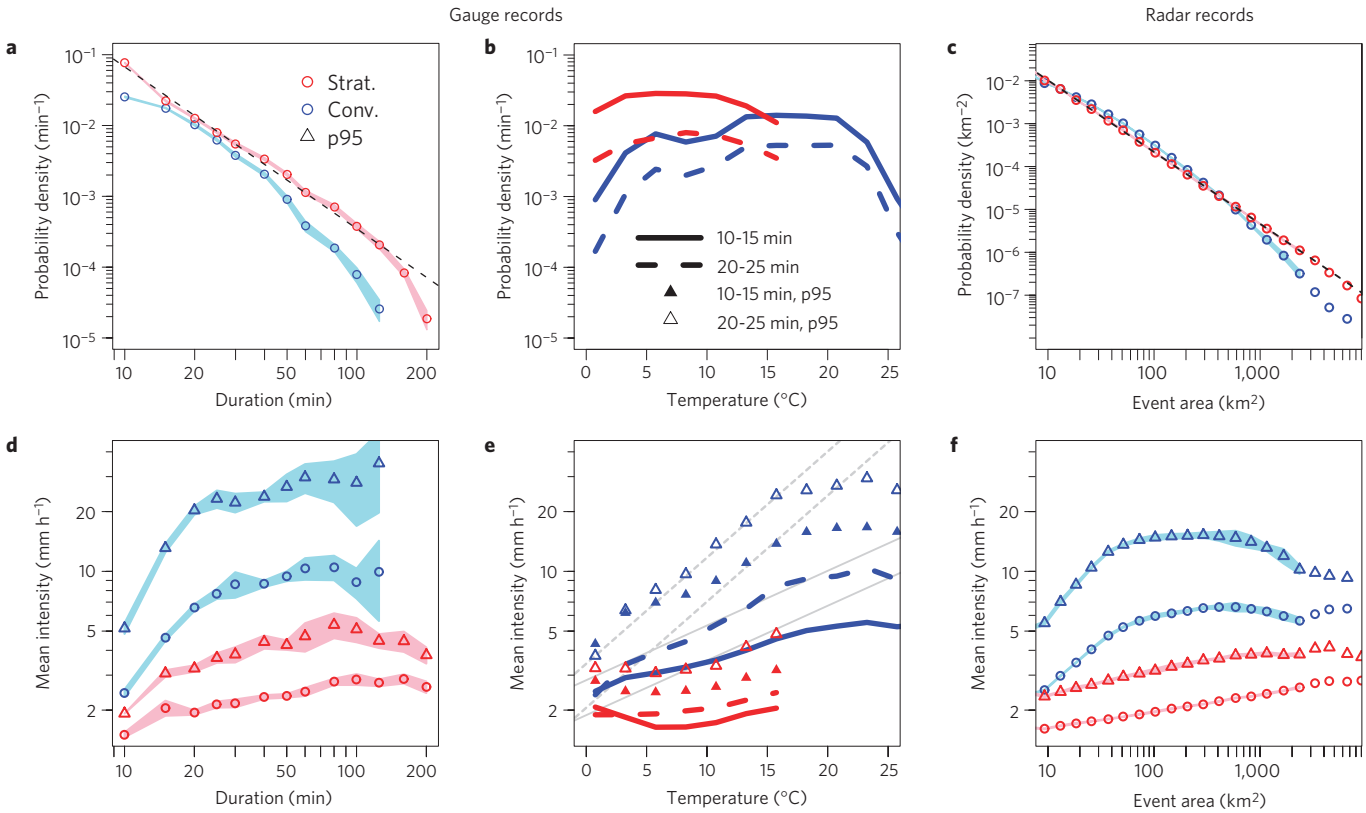

Figure 4 | Event scaling in time and space. Characteristics of convective (blue) and stratiform (red) events for gauges (left and central column) and radar (right). **a**, Distributions of event duration. Dashed line indicates power-law fit. **b**, Temperature dependence of event occurrence conditional on duration. **c**, The same as **a** for event area. **d**, Duration dependence for average (circles) and extreme events (95th percentile, triangles). **e**, Temperature dependence of average (lines) and extreme events (triangles) conditional on duration. Solid and dashed lines indicate 7% $°C^{-1}$ and 14% $°C^{-1}$ increases, respectively. **f**, The same as for **d** for event area. Note the vertical (horizontal) log-scales in all panels (left and right columns).

A simple mechanism driving observed intensity increases has recently been sought in a comparison with humidity records[7,8]. Conditioning measurements of near-surface humidity on precipitation records (Supplementary Fig. S8), we find nearly constant relative humidity as a function of temperature for stratiform conditions, and hence, indeed, an exponential increase of saturation humidity with temperature. Notwithstanding the limitations of using surface observations[7], specific humidity increases together with the overall featureless spatial structure (Fig. 4) may point to a sufficient explanation of intensity changes from thermodynamics alone. Conversely, for convection, there is a clear overall decrease in relative humidity with temperature. Along with the observed marked intensity increases (Figs 2c and 4e), this could imply that, in fact, convective dynamics react sensitively to changes in temperature. Reduced moisture availability could partially account for a possible levelling-off of precipitation intensities for very high temperatures[7] (compare also Figs 2c and 4e above 22 °C). However, even here, a scale set by the dynamics, not thermodynamics, should be investigated.

Considerable observational agreement on precipitation extremes in distinct climate zones has recently been attained[7–9], indicating common physical processes. Our results point towards a physical picture where convective plumes entrain more moist air from the surrounding atmosphere as temperature rises[1,10]. Future research should focus on the modelling of precipitating convective updrafts to capture the three-dimensional moisture and energy fluxes as a function of temperature for single[10] and multiple cells[25]. Observational constraints on present-day precipitation variability[26] have been suggested to narrow the spread of model predictions of precipitation under climate change[27]. The high-resolution data used here span a large range of spatial and temporal scales, which is needed to characterize convective precipitation statistics. Thus, our results may serve as a benchmark for operational weather forecasting as well as global climate models through more adequate descriptions of convective processes.

Methods

The three-hourly synoptic cloud observations over Germany were taken from the Met Office Integrated Data Archive System database (http://badc.nerc.ac.uk/view/badc.nerc.ac.uk__ATOM__dataent_ukmo-midas). At each synoptic station (Fig. 1a) convective-type precipitation is associated with class C for observations of cumulus- and cumulonimbus-type clouds, and stratiform precipitation with class S for observations of stratus and nimbostratus clouds. Co existence of the two types at a single location is classified as mixed (M). As the synoptic conditions, observed every three hours, can change with time, the data are aggregated over the study region divided into quadrants (Fig. 1a). The entire quadrant is at any time step assigned an overall classification termed *Q1* for occurrences of C or S respectively within the quadrant (simultaneous occurrences of the two types are not considered in the analysis), or *Q2* with the additional stricter criterion that there are more C, respectively S, records than M records in the quadrant. For example, in Fig. 1b, the northeastern quadrant fulfils both the *Q1* and the *Q2* criterion for the stratiform type. The other quadrants do not fulfil either of the criteria because both types (C and S) are present there. We apply both criteria for all analyses. *Q2* was generally found to yield the best balance between sample size and clear separation for events (Figs 3, 4 and Supplementary Fig. S4). Instantaneous intensity distributions were produced using *Q1* (Fig. 2 and Supplementary Fig. S2) and *Q2* (Supplementary Fig. S3). Our method enables us to obtain spatially homogeneous classification from many independent observers. The synoptic conditions are assumed not to change during the 90 min before and after the observation (see Supplementary Information). The synoptic observations were carried out by human observers, and are therefore subject to visibility conditions. Such effects, and a comparison with

the traditional bright-band classification[12,13] (Supplementary Fig. S5), are explored in the Supplementary Information.

The gauge data are of the ombrometer type using the weighting principle. Their accuracy is between 0.01 and 0.1 mm; the latter was used in the analysis for reasons of compatibility. Data for the period April 1997 to December 2004 were used, and stations with more than 10% missing 5 min intervals were removed from the analysis. The data were previously thoroughly quality checked, and further checks for outliers showed the data to be of high quality. Precipitation events were retrieved from the data by counting continuous times of precipitation larger than the accuracy (0.1 mm). For each event, we calculated statistics of event duration, mean intensity, mean and maximum temperature (from E-OBS (ref. 28), http://www.ecad.eu/download/ensembles/ensembles.php) at the day the event took place.

The RY radar data product was provided by the General Observation Period project[29]. It is a 1 km × 1 km grid composite of 17 radar measurement facilities (Fig. 1a) for the two-year time period 2007–2008. Rainfall rates (R) were derived from raindrop reflectivities (Z) using the Z–R relationship[30]. Discrete instantaneous precipitation intensities, in units of 0.1 mm h^{-1}, are provided. We derive two data packages from the original data: the total and temperature-conditional intensity distributions, using daily mean and maximum temperatures from the E-OBS data with 1 °C bin size; an algorithm was constructed that detects connected precipitating areas with an intensity of at least 1.2 mm h^{-1}. Statistics of event area, the area-integrated intensity, the maximum intensity of each connected event, the distribution of intensities within each event, and the daily mean and maximum temperature at the location of the areal centre of mass of the event were calculated. A cutoff of 1.2 mm h^{-1} was applied to make the radar data compatible with the gauge data, which have a lower cutoff of 0.1 mm per 5 min (1.2 mm h^{-1}). To avoid boundary effects, cells with centre of mass closer than 50 km to the boundary of the radar data (Fig. 1a) are removed from the statistics. For comparison with the gauge data we restrict the study domain to southern Germany, but results are rather insensitive to shifts of the domain.

A number of sensitivity tests were carried out for both the gauge and radar analysis and the results were found to be robust with respect to the conclusions drawn (see Supplementary Information).

Statistical tests were calculated with a bootstrapping method, with surrogate data sets produced by sub-sampling independent data blocks with half the sample of the original data. Shaded areas in the figures denote the 90% confidence interval. The units of the vertical axes in Figs 2a, 3a–c and 4a,c are obtained by the normalization of probability density.

Received 25 July 2012; accepted 15 January 2013; published online 17 February 2013

References

1. Trenberth, K. E., Dai, A., Rasmussen, R. M. & Parsons, D. B. The changing character of precipitation. *Bull. Am. Meteorol. Soc.* **84,** 1205–1217 (2003).
2. Allan, R. P. & Soden, B. J. Atmospheric warming and the amplification of precipitation extremes. *Science* **321,** 1481–1484 (2008).
3. Allen, M. R. & Ingram, W. J. Constraints on future changes in climate and the hydrologic cycle. *Nature* **419,** 224–232 (2002).
4. Lenderink, G. & van Meijgaard, E. Increase in hourly precipitation extremes beyond expectations from temperature changes. *Nature Geosci.* **1,** 511–514 (2008).
5. Lenderink, G., van Meijgaard, E. & Selten, F. Intense coastal rainfall in the Netherlands in response to high sea surface temperatures: Analysis of the event of August 2006 from the perspective of a changing climate. *Clim. Dynam.* **32,** 19–33 (2009).
6. Haerter, J. O., Berg, P. & Hagemann, S. Heavy rain intensity distributions on varying timescales and at different temperatures. *J. Geophys. Res.* **115,** D17102 (2010).
7. Hardwick Jones, R., Westra, S. & Sharma, A. Observed relationship between extreme sub-daily precipitation, surface temperature and relative humidity. *Geophys. Res. Lett.* **37,** L22805 (2010).
8. Lenderink, G., Mok, H. Y., Lee, T. C. & van Oldenborgh, G. J. Scaling and trends of hourly precipitation extremes in two different climate zones—Hong Kong and the Netherlands. *Hydrol. Earth Syst. Sci.* **15,** 3033–3041 (2011).
9. Utsumi, N., Seto, S., Kanae, S., Maeda, E. E. & Oki, T. Does higher surface temperature intensify extreme precipitation? *Geophys. Res. Lett.* **38,** L16708 (2011).
10. Singleton, A. & Toumi, R. Super-Clausius–Clapeyron scaling of rainfall in a model squall line. *Q. J. R. Meteorol. Soc.* http://dx.doi.org/10.1002/qj.1919 (2012).
11. Berg, P. & Haerter, J. Unexpected increase in precipitation intensity with temperature—a result of mixing of precipitation types? *Atmos. Res.* **119,** 56–61 (2013).
12. Steiner, M., Houze, R. A. Jr & Yuter, S. E. Climatological characterization of three-dimensional storm structure from operational radar and rain gauge data. *J. Appl. Meteorol.* **34,** 1978–2007 (1995).
13. Houze, R. Jr Stratiform precipitation in regions of convection: A meteorological paradox? *Bull. Am. Meteorol. Soc.* **78,** 2179–2226 (1997).
14. Haerter, J. O. & Berg, P. Unexpected rise in extreme precipitation caused by a shift in rain type? *Nature Geosci.* **2,** 372–373 (2009).
15. Romps, D. M. Response of tropical precipitation to global warming. *J. Atmos. Sci.* **68,** 123–138 (2011).
16. Muller, C. J., O'Gorman, P. A. & Back, L. E. Intensification of precipitation extremes with warming in a cloud-resolving model. *J. Clim.* **24,** 2784–2800 (2011).
17. O'Gorman, P. A. & Schneider, T. Scaling of precipitation extremes over a wide range of climates simulated with an idealized GCM. *J. Clim.* **22,** 5676–5685 (2009).
18. Wilcox, E. M. & Donner, L. J. The frequency of extreme rain events in satellite rain-rate estimates and an atmospheric general circulation model. *J. Clim.* **20,** 53–69 (2007).
19. Kharin, V. V., Zwiers, F. W., Zhang, X. & Hegerl, G. C. Changes in temperature and precipitation extremes in the IPCC ensemble of global coupled model simulations. *J. Clim.* **20,** 1419–1444 (2007).
20. O'Gorman, P. & Schneider, T. The physical basis for increases in precipitation extremes in simulations of 21st-century climate change. *Proc. Natl Acad. Sci. USA* **106,** 14773–14777 (2009).
21. Coumou, D. & Rahmstorf, S. A decade of weather extremes. *Nature Clim. Change* 1–6 (2012).
22. Von Hardenberg, J., Ferraris, L. & Provenzale, A. The shape of convective rain cells. *Geophys. Res. Lett.* **30,** 2280 (2003).
23. Rebora, N. & Ferraris, L. The structure of convective rain cells at mid-latitudes. *Adv. Geosci.* **7,** 31–35 (2006).
24. Zepeda-Arce, J., Foufoula-Georgiou, E. & Droegemeier, K. K. Space–time rainfall organization and its role in validating quantitative precipitation forecasts. *J. Geophys. Res.* **105,** 10129–10146 (2000).
25. Feingold, G., Koren, I., Wang, H., Xue, H. & Brewer, W. A. Precipitation-generated oscillations in open cellular cloud fields. *Nature* **466,** 849–852 (2010).
26. Liu, C. & Allan, R. P. Multisatellite observed responses of precipitation and its extremes to interannual climate variability. *J. Geophys. Res.* **117,** D03101 (2012).
27. O'Gorman, P. A. Sensitivity of tropical precipitation extremes to climate change. *Nature Geosci.* **5,** 697–700 (2012).
28. Haylock, M. R. *et al.* A European daily high-resolution gridded data set of surface temperature and precipitation for 1950–2006. *J. Geophys. Res.* **113,** D201192 (2008).
29. Crewell, S. *et al.* The general observation period 2007 within the priority program on quantitative precipitation forecasting: Concept and first results. *Meteorol. Z.* **17,** 849–866 (2008).
30. Steiner, M., Smith, J. A. & Uijlenhoet, R. A microphysical interpretation of radar reflectivity-rain rate relationships. *J. Atmos. Sci.* **61,** 1114–1131 (2004).

Acknowledgements

The authors acknowledge the radar and gauge data from the German Weather Service (DWD), synoptic codes from the Met Office Integrated Data Archive System, retrieved through the British Atmospheric Data Centre (BADC), and the E-OBS data set from the EU-FP6 project ENSEMBLES (http://ensembles-eu.metoffice.com) and the data providers in the ECA&D project (http://eca.knmi.nl), as well as the Cloudnet project (EU contract EVK2-2000-00611) for providing the Lindenberg Level 1 observational data. P.B. acknowledges support from the Center for Disaster Management and Risk Reduction Technology (CEDIM) through IMK-TRO. J.O.H. acknowledges support by the Danish National Research Foundation through the Center for Models of Life.

Author contributions

P.B. processed the synoptic and station data, performed data analysis and contributed to the manuscript. C.M. performed the preparation of the radar data and contributed to the manuscript. J.O.H. performed the radar data analysis and contributed to the manuscript. The initial idea was equally conceived by P.B. and J.O.H.

Additional information

Supplementary information is available in the online version of the paper. Reprints and permissions information is available online at www.nature.com/reprints. Correspondence and requests for materials should be addressed to J.O.H.

Competing financial interests

The authors declare no competing financial interests.